Novel Method for Measuring the Adhesion Energy of Vesicles

Thomas Gruhn,* Thomas Franke,† Rumiana Dimova, and Reinhard Lipowsky

Max Planck Institute of Colloids and Interfaces, Science Park Golm, 14424 Potsdam, Germany

Received October 25, 2006. In Final Form: January 18, 2007

Adhering vesicles with osmotically stabilized volume are studied with Monte Carlo simulations and optical microscopy. The simulations are used to determine the dependence of the adhesion area on the vesicle volume, the surface area, the bending rigidity, the adhesion energy per membrane area, and the adhesion potential range. The simulation results lead to a simple functional expression that is supplemented by a correction term for gravity effects. The obtained equation provides a new tool to analyze optical microscopy data and, thus, to measure the adhesion energy per area by analyzing the geometry of the adhering vesicle. The method can be applied in the weak and ultra-weak adhesion regime, where the adhesion energy per area is below 10^{-6} J/m^2. By comparing the shapes of adhering vesicles with different reduced volumes, the bending rigidity can be estimated as well. The new approach is applied to experimental data for lipid vesicles on (i) an untreated and (ii) a monolayer-coated glass surface, providing ultra-weak and weak adhesion strength, respectively.

Introduction

All forms of life are based on the principle of screening small spatial regions from the chemical conditions of the surrounding.[1] Living cells are enclosed by a lipid membrane that is impermeable for most larger molecules. On the other hand, lipid membranes can be penetrated by water molecules and due to their fluidity they can adapt to steric constraints imposed by the environment.[2] Many mechanical and chemical membrane properties can also be studied on vesicles, which solely consist of a closed lipid membrane. In spite of their comparably simple composition, vesicles allow the study of phenomena like budding transitions,[3,4] fusion,[5] and fission.[6]

The adhesion behavior of cells and vesicles is of great relevance for a fundamental understanding of cell interaction as well as for biotechnological applications like implantation materials[7] or biosensors[8] in which cells are in contact with electrodes. In many cases it is important or even essential to know the adhesion energy per membrane area W between vesicle and substrate. There are only a few experimental methods to measure W. For vesicles aspirated by a micropipet, the adhesion energy can be extracted from the relation between the suction pressure and the corresponding adhesion area.[9,10] Since the mechanical treatment may cause a damage on the vesicle that hinders subsequent investigations, purely optical measurement techniques are preferable. Bernard et al. have used phase contrast microscopy in combination with evanescence wave-induced fluorescence microscopy to study the adhesion process of a vesicle and extracted W from the spreading dynamics of the adhesion zone.[11] The method requires an observation starting from a non-equilibrium configuration of the adhering vesicle, which is typically rather difficult to prepare. The analysis of the measurements is based on a theory for the wetting behavior of liquid droplets. The assumption of a spherical cap geometry restricts the method to large adhesion strengths, where the bending rigidity is negligible.

In a different approach, Lai et al. used cross-polarizer and reflectance interference microscopy to measure the adhesion area radius and the mid-plane diameter of an equilibrated vesicle adhering to a pure glass substrate.[12] The pure glass surface provides a weak adhesion so that the bending rigidity is relevant and the shape of the vesicle deviates significantly from that of a spherical cap.[13] Ignoring this discrepancies, one can apply an elasticity theory for spherical cap geometries to extract an estimate of the adhesion strength.[12]

The adhesion strength can roughly be divided into two regimes:[10] In the strong adhesion regime ($W > 10^{-6}$ J/m^2), bending rigidity is negligible and the vesicle has the shape of a spherical cap, which is basically determined by the membrane area and the volume of the vesicle. In the weak adhesion regime ($W < 10^{-6}$ J/m^2), the shape of the vesicle results from the interplay between adhesion and bending energy. Therefore, in the weak adhesion regime, adhesion strength and bending rigidity can be extracted from an analysis of the vesicle shape. In many experiments the vesicle adheres to an untreated, pure glass substrate. As shown in Figure 1a, the shape is far from a spherical cap geometry, indicating a low adhesion strength. The contact radius R_c, which is the radius of the vesicle contour close to the adhesion zone, is roughly of the order of 3 μm. If the bending rigidity κ is known, a first estimate of the adhesion strength can be made by using the relation $W = \kappa/(2R_c^2)$, which has been derived for vesicles adhering to a contact potential.[13] With $\kappa = 10T$, where T is the thermal energy, including the Boltzmann constant k_B, we find that the adhesion strength for a vesicle and

* Corresponding author. E-mail: gruhn@mpikg.mpg.de.

† Present address: Institut für Physik der Universität, Universitätsstr. 1, D-86159 Augsburg, Germany.

(1) Morowitz, H. J. *Beginnings of Cellular Life*; Yale University Press: London, 1992.

(2) Lipowsky, R., Sackmann, E., Eds. *Handbook of Biological Physics*; Elsevier: Amsterdam, 1995.

(3) Berndl, K.; Käs, J.; Lipowsky, R.; Sackmann, E.; Seifert, U. *Europhys. Lett.* **1990**, *13*, 659.

(4) Seifert, U.; Berndl, K.; Lipowsky, R. *Phys. Rev. A* **1991**, *44*, 1182.

(5) Haluska, C.; Riske, K.; Marchi-Artzner, V.; Lehn, J.-M.; Lipowsky, R.; Dimova, R. *Proc. Natl. Acad. Sci. U.S.A.* **2006**, *43*, 15841.

(6) Hanczyc, M. M.; Szostak, J. W. *Curr. Opin. Chem. Biol.* **2004**, *8*, 660.

(7) Turner, N.; Armitage, M.; Butler, R.; Ireland, G. *Cell Biol. Int.* **2004**, *28*, 541.

(8) Arndt, S.; Seebach, J.; Psathaki, K.; Galla, H. J.; Wegener, J. *Biosens. Bioelectron.* **2004**, *19*, 583.

(9) Evans, E.; Metcalfe, M. *Biophys. J.* **1984**, *46*, 423.

(10) Evans, E. *Langmuir* **1991**, *7*, 1905.

(11) Bernard, A.-L.; Guedeau-Boudeville, M.-A.; Jullien, L.; di Meglio, J.-M. *Langmuir* **2000**, *16*, 6809.

(12) Lai, A. C.-K.; Wan, K.-T.; Chan, V. *Biophys. Chem.* **2002**, *99*, 245.

(13) Seifert, U.; Lipowsky, R. *Phys. Rev. A* **1990**, *42*, 4768.

10.1021/la063123r CCC: $37.00
Published on Web 04/10/2007

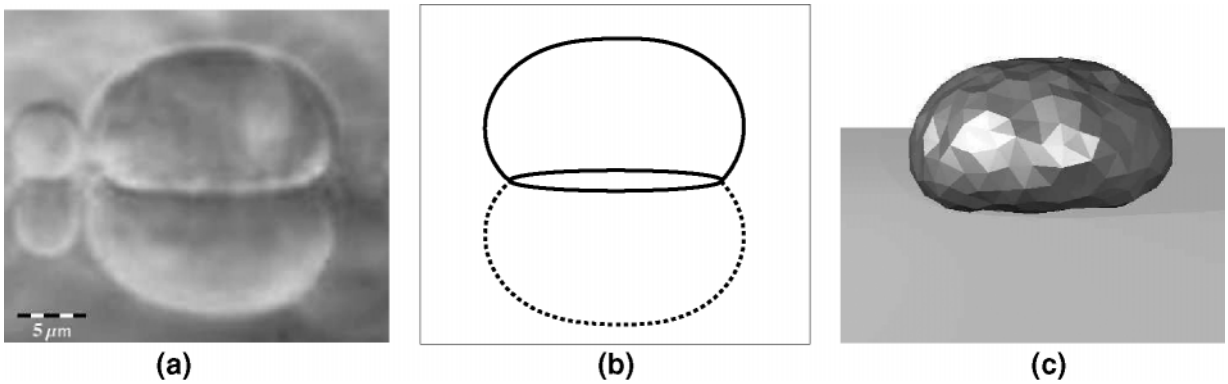

Figure 1. (a) Optical micrographs of two vesicles adhering to a pure glass substrate, which reflects the vesicle shapes. (b) From the large vesicle we extract the contour, which includes all relevant geometric properties: the total surface area, the reduced volume, and the base area. Using eq 14, the adhesion strength can be measured. The shown vesicle with a bending rigidity $\kappa \simeq 10T$ has a reduced volume $v \simeq 0.87$ and a reduced adhesion strength $w \simeq 5.8$. (c) Typical configuration from a vesicle simulation with $v = 0.9$, $w = 6.1$, and $\kappa = 10T$.

a pure glass substrate is of the order of $W \simeq 10^{-9}-10^{-8}$ J/m^2 and lies in the range of ultra-weak adhesion.

In this paper we present relations between geometrical and material properties of adhering vesicles, which are obtained from Monte Carlo simulations and analytical estimates. The derived equations can be used to analyze optical microscopy images in order to obtain the adhesion strength W. The method can be used for weak and ultra-weak adhesion strengths. Especially for ultra-weak adhesion strength, our method avoids the systematic errors arising from the assumption of a spherical cap geometry. The required experimental effort of our new method is comparably small. In a first set of experimental measurements, the new method provides reasonable results for weak and ultra-weak adhesion strengths.

In many experiments, the mass density inside the vesicle differs from that outside, which provides an effective adhesion strength modified by gravity effects. We present a correction term for these latter effects, which is typically neglected in adhesion strength measurements and turns out to be important for the case of ultra-weak adhesion. By comparing the shapes of adhering vesicles with different volumes, the bending rigidity κ can be estimated as well.

The new approach is based on a relation between the geometry and the material properties of an equilibrated adhering vesicle. For small thermal fluctuations, corresponding to the limit of low temperature T, the contour of adhering vesicles is determined by a set of differential equations that can be solved numerically.[13] At finite temperature, Monte Carlo (MC) simulations can be used to obtain equilibrium properties of adhering vesicles. Recently, we presented a simulation-based study of the adhesion of vesicles with variable volume (i.e., which do not experience any constraint on their volume).[14] In general, the volume of vesicles is influenced by so-called "osmotically active" molecules inside and outside the vesicle, which are too large to penetrate the membrane. The case of variable volume, studied in ref 14, corresponds to the absence of osmotically active molecules. If the density of osmotically active molecules inside and outside the vesicle is high, the vesicle volume V fluctuates only weakly around an equilibrium volume V_0. Many equilibrium shapes of adhering vesicles with osmotically controlled volume differ significantly from the equilibrium shapes of vesicles with variable V.

Osmotically induced volume stabilization is often applied in vesicle experiments because it resembles the conditions in biological cells and it simplifies the shape analysis. In the present study, the adhesion behavior of thermally fluctuating vesicles with an osmotically stabilized volume is investigated systematically for the first time, using a set of 400 extensive MC simulations. A priori, no assumptions are made about the shape or the symmetry properties of the vesicle. The observations are used to derive a functional relation between the adhesion area, the vesicle volume, the bending rigidity of the membrane, the adhesion strength, and the adhesion potential range.

In addition, this paper also describes the results of a first set of experimental observations in which contour images of 17 adhering vesicles have been measured with optical microscopy. Two types of substrates have been chosen in order to realize weak and ultra-weak adhesion strength. Images of the adhering vesicles have been analyzed with the help of the simulation-based relations (see Figure 1). The analysis provides values for the adhesion strengths and an estimate of the bending rigidity.

Geometric Membrane Model

The simulations are based on the geometric membrane model discussed in ref 13. We assume that the spontaneous curvature M_0 is negligibly small and that the Gaussian curvature is not relevant since the vesicle does not change its topology. Then the elastic curvature energy E_{el} and the adhesion energy E_{ad} can be expressed as:[13]

$$E_{el} + E_{ad} \equiv \frac{\kappa}{2}\int_{S_{ves}} dA(2M)^2 - WA_{ad} \qquad (1)$$

where S_{ves} is the vesicle surface, κ is the bending rigidity, and M is the local mean curvature. The adhesion potential between a planar homogeneous substrate and a vesicle is approximated by a square-well potential, which is defined by its potential range d and its adhesion energy $W > 0$ per membrane area. The adhesion area A_{ad} is defined by those membrane patches that have a separation l with $l < d$ from the substrate surface.

Since the lipid bilayer is permeable for water molecules, the volume V of a vesicle can change, while the number N_{in} of osmotically active particles inside the vesicle stays constant. For a sufficiently large concentration ρ_0 of osmotically active molecules outside the vesicle, the osmotic energy is given by

$$E_{os} \simeq \frac{\rho_0 T}{2V_0}(V - V_0)^2 \qquad (2)$$

with $V_0 \equiv N_{in}/\rho_0$.

During the simulation, the membrane area A is kept constant up to small fluctuations $|\Delta A| < 0.01A$, which are necessary to

(14) Gruhn, T.; Lipowsky, R. *Phys. Rev. E* **2005**, *71*, 011903.

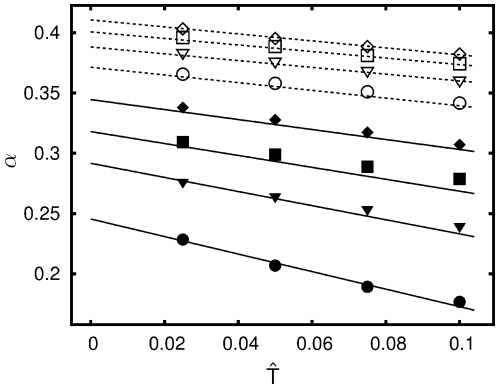

Figure 2. Relative adhesion area $\alpha = A_{ad}/A$ of an adhering vesicle with stabilized volume as a function of the rescaled temperature $\hat{T}$ for a rescaled potential range $\hat{d} = 0.06$. For the adhesion strength $w = 20$ simulation results for reduced volumes $v = 0.41$ (△), 0.49 (◇), 0.57 (□), 0.65 (▽), and 0.73 (○) are shown. For $w = 6.3$ results are shown for $v = 0.56$ (◆), 0.7 (■), 0.78 (▼), and 0.88 (●). Lines show solutions of eq 11.

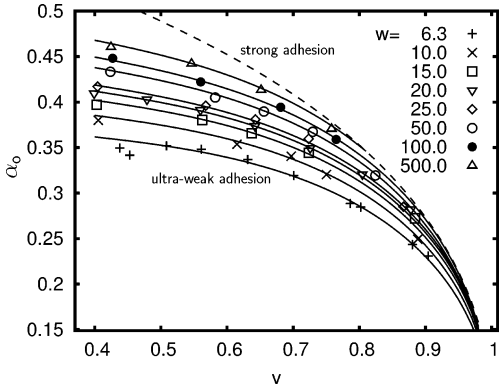

Figure 3. Relative adhesion area α_0 in the limit of temperature $T = 0$ as a function of the rescaled vesicle volume v. Values are extrapolated from results of simulations with a rescaled potential range $\hat{d} = 0.06$. Lines show the relative adhesion area of a spherical cap α_{sc} (···) and fits of α_0 (—).

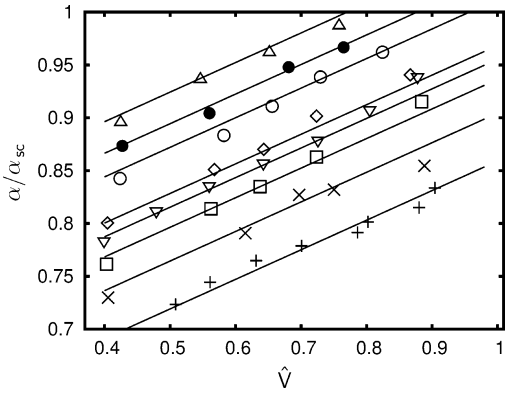

Figure 4. Quotient of the relative adhesion area $\alpha_0(\hat{V})$ in the limit of temperature $T = 0$ and the corresponding spherical cap value $\alpha_{sc}(\hat{V})$ increases nearly linearly with the rescaled vesicle volume v. The symbols correspond to the results shown in Figure 3.

sample the configuration space in an efficient way. Using κ and the length $R \equiv \sqrt{A/4\pi}$, we define the dimensionless temperature and adhesion strength quantities via

$$\hat{T} \equiv T/\kappa \tag{3}$$

and

$$w \equiv WR^2/\kappa \tag{4}$$

Furthermore, we also use the dimensionless quantities

$$\hat{d} \equiv d/R \tag{5}$$

$$v \equiv 3V/(4\pi R^3) \tag{6}$$

$$\alpha \equiv A_{ad}/A \tag{7}$$

Spherical vesicles have radius R and reduced volume $v = 1$. The molecular concentration $\rho_0 = 5 \times 10^4 R^{-3}$ is chosen small enough to ensure an adequate sampling of the configuration space. For the analysis of the simulation data, the measured equilibrium volumes v are used, which deviate less than 2% from $v_0 \equiv 3V_0/(4\pi R^3)$.

In the MC simulations, the vesicle is represented by a triangulated model system building a polygon with interconnected vertices.[15] Four hundred simulations with 1.2×10^6 MC sweeps were performed for a vesicle model with 1280 triangles, half of the sweeps were used for equilibration. Each sweep consists of 1280 tentative vertex moves and 3840 edge flip attempts. A detailed description of the simulation method is given in ref 14 for vesicles with variable volume.

Simulations were performed systematically for reduced temperatures $0.025 \le \hat{T} \le 0.1$ and volumes $0.4 \le v \le 0.925$; adhesion strength and potential range were varied in the ranges $5.0 \le w \le 500.0$ and $0.03 \le \hat{d} \le 0.09$.

Parameter Dependence of Reduced Adhesion Area α. In a first step, we investigate the temperature dependence of α, as defined in eq 7, if w, κ, d, and v_0 are fixed. Considering small fluctuation modes around the ground state of an adhering vesicle, it was predicted in ref 14 that α decreases linearly with increasing temperature T. The validity was shown for adhering vesicles with variable volume. In the new set of simulations, discussed here, we investigated the adhesion behavior for vesicles with an osmotically stabilized volume. As shown in Figure 2, the reduced adhesion area α is again linear in T so that α can be written as

$$\alpha \approx \alpha_0(v,w,\hat{d}) + \hat{T}\alpha_1(v,w,\hat{d}) \tag{8}$$

with $\alpha_1 < 0$. It is noteworthy that quantities such as κ, A, and w can depend on temperature as well. In this case, eq 6 and all other equations are still valid, but α can become a nonlinear function of T.

A linear extrapolation of α toward $\hat{T} = 0$ provides α_0 as shown in Figure 3 for $\hat{d} = 0.06$. It is instructive to compare α_0 with the relative adhesion area $\alpha_{sc}(v,\hat{d})$ of an adhering vesicle with a spherical cap geometry, which is the limiting case for large w. As shown in the Appendix, α_{sc} is determined by

$$\alpha_{sc} = \alpha_{ba} + \hat{d}\frac{1 - \alpha_{ba}^2}{2v} \tag{9}$$

where

$$\alpha_{ba} \equiv \cos\left(\frac{1}{3}\arccos(1 - 2v^2)\right) - \frac{1}{2} \tag{10}$$

is the ratio between the circular base area A_{ba} and the total area A. Figure 4 shows that α_0/α_{sc} is approximately a linear function of v. More generally, α_0/α_{sc} can be fitted by a linear expression in v, $w^{-1/2}$, and $\hat{d}$. Similarly, the coefficient α_1, as introduced in

(15) Gompper, G.; Kroll, D. M. *Phys. Rev. Lett.* **1994**, *73*, 2139.

eq 6, can be fitted by a linear combination of υ, υ^2, $w^{-1/2}$, and $\hat{d}$. As a result, one obtains

$$\alpha = \alpha_{sc} f_0 + f_1 \hat{T} - (\alpha_{sc} + 1.4\hat{T}) \frac{0.55}{\sqrt{w}} \tag{11}$$

with

$$f_0 \equiv 0.75 + 0.28\upsilon + 0.8\hat{d} \tag{12}$$

and

$$f_1 \equiv -0.8 + 2.2\upsilon(1 - \upsilon) + 2.5\hat{d} \tag{13}$$

The dependence on w is taken into account by a term proportional to $w^{-1/2}$ in analogy to the adhesion behavior of a vesicle with variable volume.[14] Equations 9−13 can now be used to determine the adhesion strength and the bending rigidity for an adhering vesicle from experimental data.

Extracting Adhesion Strength and Bending Rigidity. If κ and $\hat{d}$ are known, the adhesion energy per area W can be obtained from eq 11 as

$$\frac{WA}{4\pi\kappa} = w = \left(0.55 \frac{\alpha_{sc}\kappa + 1.4T}{(\alpha_{sc} f_0 - \alpha)\kappa + f_1 T}\right)^2 \tag{14}$$

by measuring A, A_{ad}, and V of one adhering vesicle. The largest contribution to the error δw arises from the error $\delta\alpha$ of measuring α:

$$\frac{\delta w}{w} \lesssim \frac{\partial w}{\partial \alpha} \frac{\delta \alpha}{w} = \frac{2\sqrt{w}}{0.55(\alpha_{sc} + 1.4\hat{T})} \delta\alpha \tag{15}$$

A higher accuracy for w and measurements of other quantities can be achieved by analyzing the adhesion behavior for various vesicle volumes. The vesicle volume can be controlled by the concentration ρ_0 of osmotically active molecules outside the vesicle. Alternatively, several adhering vesicles with different υ can be compared. In the following, we refer to the latter method.

We consider two adhering vesicles (1) and (2) with identical values for W, T, d, and κ. The volume of vesicle (i) is denoted by $V^{(i)}$ with $i = 1, 2$. With

$$Q^{(i)} \equiv (A^{(i)})^{-1/2} \frac{\alpha_{sc}^{(i)}\kappa + 1.4T}{(\alpha_{sc}^{(i)} f_0^{(i)} - \alpha^{(i)})\kappa + f_1^{(i)} T} \tag{16}$$

one has

$$\sqrt{\frac{W}{1.21\pi\kappa}} = Q^{(1)} = Q^{(2)} \tag{17}$$

The second equality in eq 17 is a quadratic equation in κ; since f_0, f_1, and α_{sc} are linear functions in d, it is also a cubic equation in d. If neither d nor κ is known, they can both be obtained by using eq 17 for three or more vesicles. The solutions found for d and κ can be inserted into eq 14 to obtain W.

Gravity Effects. Up to now the influence of gravity has been neglected. However, in many experiments the osmotically active molecules inside the vesicle are heavier than those outside of it so that the mass density difference $\Delta\rho_m > 0$ pushes the vesicle to the bottom substrate. This has two advantages: The different refraction indices inside and outside the vesicle amplify the contrast, and the vesicle can be found more easily, since it is located at the bottom substrate.

For simplicity, we consider $\hat{d} = 0$ and a spherical cap geometry for the vesicle. Then, the gravitational energy is given by

$$E_g = \Delta\rho_m g \int_{V_{sc}} z dV = \frac{\Delta\rho_m g}{12\pi} A(A - 2A_{ad}) \tag{18}$$

with the gravitational acceleration $g \simeq 9.81\ \mathrm{ms}^{-2}$. We now assume that A_{ad} is changed by an amount ΔA_{ad} while V is kept constant. The restriction to spherical caps leads inevitably to a small change ΔA of A, but in most cases $\Delta A/A$ is distinctly smaller than $\Delta A_{ad}/A_{ad}$. Neglecting ΔA, the change of E_g can be written as

$$\Delta E_g \simeq -W_g \Delta A_{ad} \tag{19}$$

with

$$W_g \equiv \frac{gA\Delta\rho_m}{6\pi} \tag{20}$$

in analogy with the adhesion energy E_{ad} in eq 1. This means, a small influence of gravitation acts like an extra contribution W_g to the adhesion energy. Consequently, the value for W obtained from eq 14 is a sum

$$W_{eff} = W_{ad} + W_g \tag{21}$$

of the net adhesion energy per area W_{ad} and the gravity contribution W_g. If vesicles with different values of A are compared, eq 17 must be corrected as well and now has the form:

$$\frac{W_{ad}}{1.21\pi\kappa} = (Q^{(1)})^2 - \frac{W_g^{(1)}}{1.21\pi\kappa} = (Q^{(2)})^2 - \frac{W_g^{(2)}}{1.21\pi\kappa} \tag{22}$$

Experimental Section

The approach described above is now applied to adhering giant vesicles studied by optical microscopy. We explored two adhesion strength regimes using two different substrates—with weak and with ultra-weak adhesion strength. In order to realize weak adhesion, we used the electrostatic interaction between negatively charged vesicles and positively charged surfaces.[16] The ultra-weak adhesion regime was studied with the same type of vesicles on a pure, untreated glass surface. The positively charged surfaces were prepared as described in ref 16. Briefly, glass cover slips were exposed to subsequent vapor deposition of chromium and gold of 25 nm final thickness. A self-assembled monolayer of the aminoalkanethiol $HS(CH)_{11}NH_2$ (Dojindo Molecular Technologies, Inc, USA) is formed by immersing the coated surface in 0.1 mM solution of the aminoalkanethiol for 1 h.[17] The surface becomes positively charged in aqueous solution while the non-coated glass surface is negatively charged. The negatively charged membranes of the giant vesicles were 9:1 mixtures of DOPC (dioleoylphosphatidylcholine) and DOPG (dioleoylphosphatidylglycerol) from Avanti Polar Lipids. Using the method of electroformation, the vesicles were grown in 220 mM sucrose solution and subsequently diluted in isotonic glucose solution resulting in a mass density difference of about 12.5 g/L. The vesicle solution was then transferred to an observation chamber, consisting of two glass cover slips sandwiching a Π-shaped Teflon spacer. The chamber is closed by the studied substrate (positively charged or pure untreated glass surface) that forms the bottom of the chamber. The two cover slips, sandwiching the Teflon spacer, allow side-view access into the chamber. The observation was performed with a horizontally mounted microscope in phase contrast mode. After introducing the vesicle solution in the chamber, the vesicles are allowed to settle on the studied surface located at the chamber bottom. Snapshots of

(16) Lipowsky, R.; Brinkmann, M.; Dimova, R.; Franke, T.; Kierfeld, J.; Zhang, X. *J. Phys. Condens. Matter* **2005**, *17*, S537.
(17) Zhu, M.; Schneider, M.; Papastavrou, G.; Akari, S.; Möhwald, H. *Langmuir* **2001**, *17*, 6471.

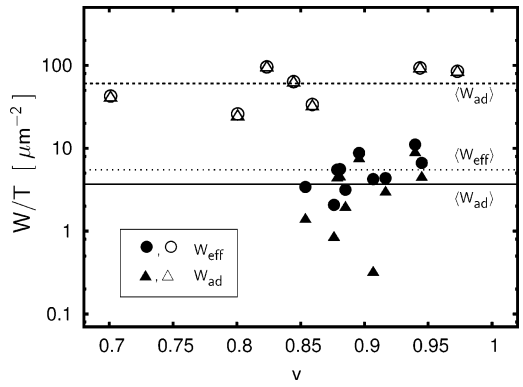

Figure 5. Effective adhesion strength W_{eff} and net adhesion strength W_{ad} divided by temperature T as functions of the rescaled volume v. Filled symbols refer to vesicles on a pure glass substrate; open symbols refer to vesicles on the substrate coated with a positively charged monolayer. Horizontal lines denote averages over the respective data points, i.e., $\langle W_{ad}\rangle$ (—) and $\langle W_{eff}\rangle$ (•••) for membranes on a pure glass substrate and $\langle W_{ad}\rangle \simeq \langle W_{eff}\rangle$ (- - -) for membranes on the coated substrate.

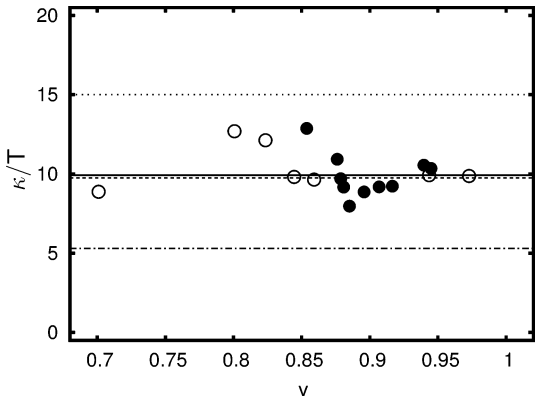

Figure 6. Bending rigidity κ divided by temperature T as a function of reduced volume v. Filled symbols refer to vesicles on a pure glass substrate, showing ultra-weak adhesion. Open symbols refer to vesicles on a weakly adhesive, coated substrate. Averages $\langle \kappa/T\rangle$ over the respective data points are denoted by horizontal lines for weak (- - -) and ultra-weak adhesion (—). Results measured in ref 24 from flickering modes (-•-•-) and electric deformation (•••) are shown for comparison.

vesicles of different sizes were taken and their contours determined. We investigated 10 vesicles on the pure glass substrate, causing ultra-weak adhesion, and 7 vesicles in contact with the weakly adhesive substrate.

Adhesion Strength. Applying eq 22 to all pairs of vesicles, optimal values for $\langle\kappa\rangle$ and $\langle d\rangle$ are determined numerically for weak and ultra-weak adhesion strength, respectively. With these values the effective adhesion energy W_{eff} and the net adhesion energy W_{ad} were obtained as shown in Figure 5. Even though the data are relatively scattered, the values for the two different substrates are clearly localized around two very distinct values of W_{eff}.

Using eq 15, we can estimate the expected spreading of the data points. For the ultra-weak adhesion we find that $\delta W_{eff}/W_{eff} \lesssim 12.5\delta\alpha/\alpha$. If α is measured with an accuracy of $\pm 5\%$, the absolute deviations of the W_{eff} data from the true value should be smaller than $\pm 63\%$, which corresponds to the observed spreading of the data points. The error range for the average value over the 10 values of W_{eff} should be smaller by a factor of $1/\sqrt{10}$, resulting in $\langle W_{eff}\rangle = 5.5T\ \mu\text{m}^{-2} \pm 1.1T\ \mu\text{m}^{-2}$. According to eq 15, the error range for W_{eff} with the weakly adhesive substrate could be four times larger than for the pure glass substrate. In practice, values of W_{eff} for the weakly adhesive substrate spread about $\pm 60\%$ around the average value. Taking this as the standard deviation, the average value for the seven weakly adhering vesicles is given by $W_{eff} = 61T\ \mu\text{m}^{-2} \pm 15T\ \mu\text{m}^{-2}$.

The data points obtained for W_{eff} and W_g are used to calculate $W_{ad} = W_{eff} - W_g$. Therefore, W_{ad} is exposed to two additional sources of error that affect W_g. On the one hand, eq 20 is based on the assumption that the influence of gravity is small, while it turns out to be comparable to the ultra-weak adhesion strength. On the other hand, the osmolarity of the external solution may be slightly different between the observed vesicles. As a general result we find that the impact of gravity is negligible for vesicles adhering to the oppositely charged monolayer while it plays an important role for the ultra-weak adhesion on pure glass.

Only a small number of previous studies have been devoted to the measurement of vesicle adhesion strength. Since there is a large number of membrane compositions and substrate materials, it is difficult to find data sets that are directly comparable. Our measurements for vesicles adhering to the oppositely charged monolayer are approximately comparable with experimental results presented in ref 11. Investigating a vesicle with a negatively charged egg−phosphatidylcholine membrane adhering to a glass substrate, coated with a positively charged indium−tin oxide monolayer, they measured the adhesion strength $W = 1.4 \times 10^{-6}$ J/m^2, which is a factor of 4−5 larger than our result for weak adhesion. Considering the different materials, it is reassuring that both results are approximately of the same order of magnitude. The same applies to the adhesion strength $W = 5 \times 10^{-9}$ J/m^2 that was found in ref 12 for a vesicle with a DMPC membrane, adhering to a pure glass substrate. Their result is a factor of 2 smaller than the adhesion strength we found for our DOPC−DOPG vesicles adhering to a pure glass substrate. Beside the different materials, one should note that the adhesion energies measured in refs 11 and 12 include effective contributions from fluctuation-induced repulsion, while in our case the pure material property W_{ad} is extracted from the fluctuating vesicle. The measured values of W are summarized in Table 1, including the range of adhesion strengths measured between two vesicles aspirated by micropipets.[10] The vesicles, which were studied in an electrolyte solution, consisted of neutral phosphatidylcholine (PC) lipids and a small amount of negatively charged phosphatidylserine (PS) lipids. Adhesion strengths in the range of 10^{-8}−10^{-5} J/m^2 were achieved by varying the charge density of the lipid membranes.

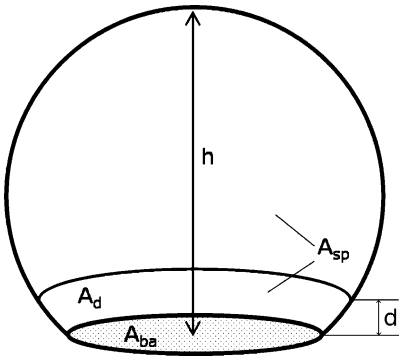

Figure 7. Spherical cap with height h, base area A_{ba}, total area $A = A_{ba} + A_{sp}$, potential range d, and adhesion area $A_{ad} = A_{ba} + A_d$. The spherical cap approximation is used to analyze the limit of negligible bending rigidity and to estimate gravity impacts on the adhesion behavior.

Bending Rigidity. By comparing several adhering vesicles with different volumes, eq 22 provides a new method to estimate the bending rigidity. In the literature, several methods for measuring κ can be found. The bending rigidity can be extracted from the thermal fluctuation spectrum of the vesicle[18] or by analyzing a vesicle aspirated into a micropipet.[19,20] Furthermore, it can be obtained from the geometry of thin lipid tethers pulled out of the vesicle

(18) Faucon, J. F.; Mitov, M.D.; Méléard, P.; Bivas, I.; Bothorel, P. *J. Phys. Fr.* **1989**, *50*, 2389.
(19) Evans, E.; Rawicz, W. *Phys. Rev. Lett.* **1990**, *64*, 2094.
(20) Rawicz, W.; Olbrich, K. C.; McIntosh, T.; Needham, D.; Evans, E. *Biophys. J.* **2000**, *79*, 328.

Table 1. Bending Rigidities and Adhesion Energies Per Area

κ/T	W [10^{-9} J/m^2]	lipid material	adhesion material	measurement technique
10	10	DOPC:DOPG (9:1)	pure glass substrate	described in this article
10	300	DOPC:DOPG (9:1)	aminoalkanethiol monolayer	described in this article
	5	DMPC	pure glass substrate	interference microscopy[12]
	1400	EPC	polylysine-coated surface	fluorescence microscopy[11]
	$10-10^4$	PC:PS (100:0−7)	second vesicle (same composition)	micropipettes[10]
	10^6	DMPC	latex sphere	optical trap[25]
5.3		DOPC		flickering spectroscopy[24]
15		DOPC		electric deformation[24]

membrane[21,22] or from the deformation of the vesicle in an external electrical field.[23]

We define the quantity

$$D_{ij} \equiv |(Q^{(i)})^2 - (Q^{(j)})^2 - \frac{W_g^{(i)} - W_g^{(j)}}{1.21\pi\kappa}| \tag{23}$$

for a pair of adhering vesicles with the same adhesion strength. According to eq 22, D_{ij} should vanish for the correct κ and d. Let N be the number of vesicles studied for the same adhesion conditions. We then look for values of κ and d which minimize the expression

$$\sum_{i=1}^{N}\sum_{j=1}^{N} D_{ij} \tag{24}$$

We have applied this method to the sets of adhering vesicles with weak and ultra-weak adhesion strength, separately. In both cases we obtained an optimal bending rigidity $\langle\kappa\rangle = 10T \pm 2T$.

In order to get more detailed information, we considered values $\kappa(i)$ that minimize the quantity $D_i = \sum_{j=1}^{N} D_{ij}$, which predominantly depends on the properties of vesicle i. In Figure 6, the resulting values of $\kappa(i)$ are shown as a function of the reduced volume v of vesicle i. Inspection of this figure reveals a certain tendency for κ to be more accurate if the reduced volume of the vesicles is large.

The bending rigidity of DOPC has been measured with two different methods by Niggemann et al.[24] From fluctuation mode spectroscopy a value $\kappa = 5.3T \pm 0.6T$ was found for a vesicle with a radius $R = 12\ \mu$m. For the same vesicle the analysis of the shape deformations induced by an electric field revealed $\kappa = 15T \pm 1.2T$. As shown in Figure 6, our results for κ obtained for vesicles with $R \simeq 10\ \mu$m lie clearly between the fluctuation mode and the electric deformation measurement.

Conclusions

With the help of Monte Carlo simulations, we have found a relation between the material properties of an adhering vesicle and geometric quantities that can be determined from the vesicle contour. Our approach provides a new optical method to measure the adhesion strength from the equilibrium shape of the adhering vesicle. This approach takes thermal fluctuations into account and is not restricted to vesicles with a spherical cap geometry. A correction term for gravity effects is included. The method is dedicated to measurements of weak and ultra-weak adhesion strengths (i.e., for adhesion strengths $W < 10^{-6}$ J/m^2).

The method is tested for a set of vesicles adhering to substrates with weak and ultra-weak adhesion strength. Results are of the same order as those found elsewhere for similar materials. The error related to individual measurements, which is inherent in our method (see eq 15), can be overcome by analyzing a larger number of vesicles, which is facilitated by the comparably low experimental effort of the method. A comparison of adhering vesicles with different volumes gives an estimate of the bending rigidity κ without any additional measurements. It will be interesting to apply our method to vesicles with cholesterol, which is known to substantially increase the bending stiffness of lipid membranes. Work in this direction is in progress.

Appendix: Spherical Cap Geometry

In the following, some geometrical properties of the spherical cap are analyzed in order to prove eqs 9 and 10, which provide a relation between the reduced adhesion area α_{sc} and the reduced volume v for a vesicle with a spherical cap geometry.

We consider a spherical cap with a volume V and a surface area A that lies on a substrate with its circular base area A_{ba} (Figure 7). The spherical part of the surface $A_{sp} = A - A_{ba}$ has a curvature radius denoted with R_{sp}, while the height (i.e., the smallest diameter) of the spherical cap is called h. We start from the following simple geometric relations for a spherical cap:

$$A = 2A_{ba} + \pi h^2 \tag{25}$$

$$V = \frac{h}{6}(3A_{ba} + \pi h^2) \tag{26}$$

$$A_{sp} = 2\pi R_{sp} h = A_{ba} + \pi h^2 \tag{27}$$

For an adhesion potential of range d the adhesion area of the spherical cap is given by

$$A_{ad} = A_{ba} + A_d \tag{28}$$

where A_d is the part of A_{sp} that is closer to the substrate than d (see Figure 7). From eq 27 it follows that

$$A_d = 2\pi R_{sp} d = A_{sp}\frac{d}{h} \tag{29}$$

where we assume that $d < h$. The aim is to express the reduced adhesion area

$$\alpha_{sc} \equiv \alpha_{ba} + \alpha_d \equiv \frac{A_{ba}}{A} + \frac{A_d}{A} \tag{30}$$

as a function of the reduced volume

$$v \equiv VV_R^{-1} \equiv V\left(\frac{4}{3}\pi R^3\right)^{-1} \tag{31}$$

with $R \equiv (A/4\pi)^{1/2}$. For convenience we introduce

$$q \equiv \frac{\pi h^2}{A} = \frac{h^2}{4R^2} \tag{32}$$

(21) Bo, L.; Waugh, R.E. *Biophys. J.* **1989**, *55*, 509.
(22) Cuvelier, D.; Imre Derényi, Bassereau, P.; Nassoy, P. *Biophys. J.* **2005**, *88*, 2417.
(23) Kummrow, M.; Helfrich, W. *Phys. Rev. A* **1991**, *44*, 8356.
(24) Niggemann, G.; Kummrow, M.; Helfrich, W. *J. Phys. II Fr.* **1995**, *5*, 413.
(25) Dietrich, C.; Angelova, M.; Pouligny, B. *J. Phys. II Fr.* **1997**, *7*, 1651.

so that V and V_R can be rewritten as

$$V = \frac{h}{12}(6A_{ba} + 2\pi h^2) \tag{33}$$

$$= \frac{h}{12}(3A - \pi h^2) = \frac{hA}{12}(3 - q) \tag{34}$$

$$V_R = \frac{\pi h^3}{6q^{3/2}} \tag{35}$$

and v can be expressed as a function of q:

$$v = \frac{V}{V_R} = \frac{Aq\sqrt{q}}{2\pi h^2}(3 - q) \tag{36}$$

$$= \frac{(3 - q)\sqrt{q}}{2} \tag{37}$$

From eq 25, it follows that

$$A_{ba} = \frac{A - \pi h^2}{2} \tag{38}$$

$$\alpha_{ba} = \frac{A_{ba}}{A} = \frac{1 - q}{2} \tag{39}$$

$$q = 1 - 2\alpha_{ba} \tag{40}$$

which provides a relation between v and α_{ba}:

$$v = (1 - \alpha_{ba})\sqrt{1 - 2\alpha_{ba}} \tag{41}$$

$$v^2 = 1 - 3\alpha_{ba}^2 - 2\alpha_{ba}^3 \tag{42}$$

The cubic equation in α_{ba} has the solution

$$\alpha_{ba} = \cos\left(\frac{1}{3}\arccos(1 - 2v^2)\right) - \frac{1}{2} \tag{43}$$

Now an expression for α_d is needed:

$$\alpha_d = \frac{A_d}{A} = \frac{A_{sp}}{A}\frac{d}{h} = \frac{A_{ba} + \pi h^2}{A}\frac{\hat{d}R}{h} \tag{44}$$

$$= \left(\frac{1 - q}{2} + q\right)\frac{\hat{d}h}{2h\sqrt{q}} \tag{45}$$

$$= \hat{d}\frac{1 + q}{4\sqrt{q}} \tag{46}$$

Multiplying eqs 37 and 46 provides

$$v\alpha_d = \hat{d}\frac{(3 - q)(1 + q)}{8} \tag{47}$$

$$= \hat{d}\frac{(2 + 2\alpha_{ba})(2 - 2\alpha_{ba})}{8} \tag{48}$$

$$\alpha_d = \hat{d}\frac{1 - \alpha_{ba}^2}{2v} \tag{49}$$

so that α_{sc} is given by

$$\alpha_{sc} = \alpha_{ba} + \hat{d}\frac{1 - \alpha_{ba}^2}{2v} \tag{50}$$

Equations 43 and 50 are identical to eqs 10 and 9.

LA063123R